

SCIENTIFIC REPORTS

OPEN

Enhanced weathering as a trigger for the rise of atmospheric O₂ level from the late Ediacaran to the early Cambrian

Wei-Ping Li¹, Yan-Yan Zhao^{2,3}, Ming-Yu Zhao⁴, Xiang-Ping Zha¹ & Yong-Fei Zheng¹

A shift toward a higher oxygen level in both ocean and atmosphere systems during the late Ediacaran to the early Cambrian has been suggested from multiple indirect proxies. However, the mechanism and magnitude of this oxidation remain unclear. To solve this issue, we measured carbon isotopes in both carbonate and organic matter as well as their trace element compositions for an Ediacaran-Cambrian sequence in the Lower Yangtze basin, South China. The $\delta^{13}\text{C}_{\text{org}}$ and $\delta^{13}\text{C}_{\text{carb}}$ excursions of this sequence are coupled and can be compared with contemporaneous global carbon isotope curves. A 2‰ rise in $\Delta^{13}\text{C}_{\text{carb-org}}$ occurred from the late Ediacaran to the early Cambrian, suggesting a substantial increase in atmospheric oxygen level from 16% to 30% of the present atmospheric level (PAL). Furthermore, the distribution pattern of rare earth elements and the concentrations of water-insoluble elements in the carbonates indicate a sudden enhancement in chemical weathering of the continental crust during the early Cambrian, which may be a trigger for the rise of atmospheric O₂ level. Both the supply of a large amount of nutrients due to the enhanced continental weathering and the contemporary increase of atmospheric oxygen concentrations may have promoted the appearance of large metazoans in the early Cambrian.

Fluctuations in atmospheric oxygen (O₂) and seawater redox play a fundamental role in driving biological evolution throughout the geological time^{1,2}. Atmospheric and seawater dissolved oxygen levels increase during the growth of organic carbon reservoirs because the CO₂ flux into the atmosphere–ocean system is balanced by carbon burial with the release of oxygen^{3,4}. The Cambrian bioradiation is thought to have occurred when the dissolved oxygen concentrations in the seawater exceed the relatively high oxygen requirements of animals⁵. Although multiple lines of evidence demonstrate a short-lived return to widespread seawater anoxia at the Ediacaran-Cambrian (E-C) boundary^{6–12}, evidence from sedimentary Mo concentrations^{5,13,14} and isotopes¹⁵, U isotopes^{16,17} and rare earth element concentrations¹⁸ demonstrates that the global seawater became progressively oxygenated in the early Cambrian^{13,15,17,19–21}. The mechanism and magnitude of raising atmospheric oxygen concentrations, however, remain to be fundamental yet unresolved questions.

A rise in atmospheric oxygen concentrations can lead to chemical changes in the Cambrian seawater and trigger the metazoan evolution^{15,22–25}. However, the high level of atmospheric oxygen alone cannot explain the rapid rise in the biological complexity of Cambrian age²⁶. The supply of essential nutrients, such as P, Ca, Fe, Na⁺, K⁺ and Mo, were also considered to have exerted a significant control on the evolution of myriad life forms^{21,27,28}. It has been suggested that a suddenly enhanced weathering of the continental crust during the E-C transition acted as a trigger for the rise in atmospheric oxygen concentrations^{29–31}. The enhanced weathering and the rise of O₂ may pave the way for the development of large and complex Cambrian animals. Here, we present the geochemical proxies of carbonates, such as the carbon isotope compositions, rare earth elements (REE + Y) distribution

¹CAS Key Laboratory of Crust-Mantle Materials and Environments, School of Earth and Space Sciences, University of Science and Technology of China, Hefei, 230026, China. ²Key Laboratory of Submarine Geosciences and Prospecting Techniques, Ministry of Education, Institute for Advanced Ocean Study, College of Marine Geosciences, Ocean University of China, Qingdao, 266100, China. ³Laboratory for Marine Mineral Resources, Qingdao National Laboratory for Marine Science and Technology, Qingdao, 266237, China. ⁴Department of Geology and Geophysics, Yale University, New Haven, Connecticut, 06511, USA. Correspondence and requests for materials should be addressed to Y.-Y.Z. (email: yanyanzhao@ouc.edu.cn) or Y.-F.Z. (email: yfzheng@ustc.edu.cn)

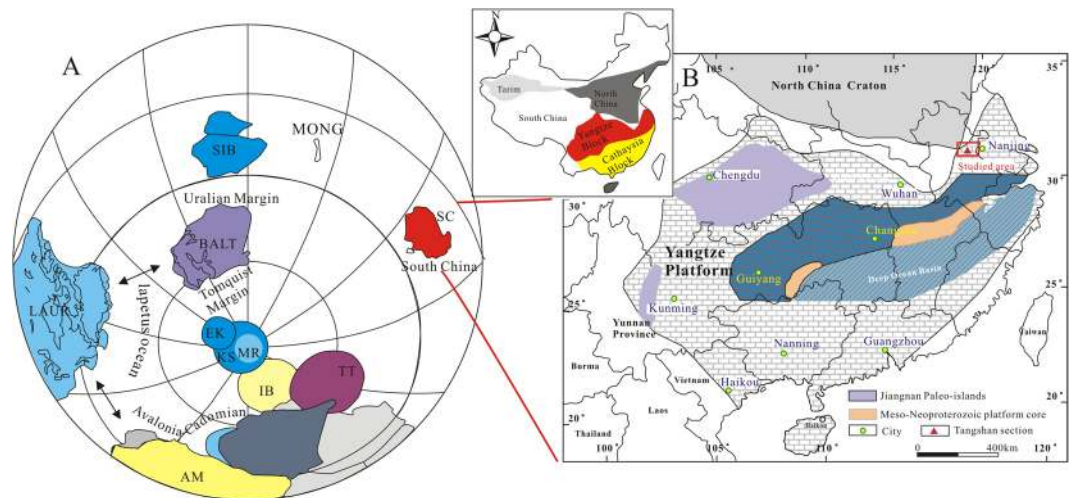


Figure 1. (A) Tentative paleogeographic reconstruction for ca. 542 Ma (modified after Maloof *et al.*³³). Cratons are labeled: LAUR—Laurentia, AM—Amazonia, WA—West Africa, BALT—Baltica, SIB—Siberia, MONG—Mongolia, and SC—South China. (B) Depositional environments during the Ediacaran–Cambrian transition on the Yangtze platform and geological settings of the Tangshan section at Chaohe in eastern Anhui, South China (modified after Li *et al.*⁴⁰). The insert map is the location of Yangtze platform and Cathaysia foldbelt. Red box and triangle denote the studied area and sample section, respectively.

patterns and water-insoluble element concentrations, to track the mechanism and magnitude of atmospheric oxygen fluctuation during the early Cambrian.

The target carbonates were sampled from an Ediacaran–Cambrian sequence at the Tangshan section in the Lower Yangtze basin, South China (Fig. 1). This region belongs to part of the Jiangnan orogen that is located between the Yangtze platform in the northwest and the Cathaysia foldbelt in the southeast³². During the E–C transition, the Yangtze platform was located at low to middle latitudes in the Northern Hemisphere (Fig. 1A)³³. It was evolved from a passive continental margin basin in the early Neoproterozoic to a series of rift basins in the middle Neoproterozoic, with a continental shelf to a marine basin from the northwest to the southeast³². The carbonate platform was surrounded by narrow marginal transitional zones to the north (~800 km long) and to the southwest (>1600 km long)^{9,34,35}, along which shallow-water carbonates sharply change into basinward black chert/shale successions^{35–37}. These sedimentary sequences on the continental shelf are characterized by repeated transgression–regression events³⁶. The post-Fortunian lower Cambrian on the Yangtze platform, from the shelf (i.e. Xiaotan, Shantan, Jinsha and Weng’an) to the slope (i.e. Songtao and Longbizui), started with black shale with similar lithologic markers or/and the first appearance of the trilobite *T. niutitangensis*^{9,38}.

The Tangshan section is located in the eastern Anhui of South China (Fig. 1B). The strata there were deposited in a restricted shallow water³⁹. From the bottom to the top (Fig. 2), the strata are composed of the Dengying Formation (DY) of the late Ediacaran, and the Lengquanwang Formation (LQW), the Bantang Formation (BT) and the Shanaoding Group (SAD) of the Cambrian⁴⁰. Small shelly fossils, including *Anabarites*, have been found at the base of the LQW Formation, indicating that the E–C boundary is roughly between the DY and LQW formations.

The Lower Cambrian strata in South China are poorly dated by isotope geochronology. The highly metalliferous black shales with high Ni–Mo concentrations from the Niutitang and Xiaoyanxi formations was once considered as close to the E–C boundary, but recent radiometric ages of 539.4 ± 2.9 Ma⁴¹, 532.3 ± 0.7 Ma⁴² and 536.3 ± 5.5 Ma³⁴ from ash beds below the highly metalliferous black shales indicate that they are younger than the E–C boundary at 541.0 ± 1.0 Ma. The onset of the globally negative $\delta^{13}\text{C}$ excursion at the lowermost Cambrian strata starts at the top of the Dengying Formation, referred to as the Basal Cambrian C-isotope Excursion (BACE)^{43–46}, was constrained at 541.00 ± 0.13 Ma in Oman^{47,48}.

Results

Petrographic observations indicate that most samples on the Tangshan section consist of microcrystalline dolomite with Mg/Ca ratios higher than 0.7¹⁹. The dolostones show minor to dense packing equigranular and anhedral crystals under a microscope and in SEM images (Fig. 3a,b), indicating primary dolomite textures without significant alteration and metamorphism. Few samples with Mg/Ca ratios lower than 0.7 (Supplementary Table S1) are composed of both calcite and dolomite, as indicated by XRD measurement (Fig. 4). In addition, the SEM image of Sample 12CH128 with a Mg/Ca ratio of 0.38 shows a calcite assemblage among the dolomite grains (Fig. 3c,d), indicating dedolomitization during burial diagenesis.

Variations in $\delta^{13}\text{C}_{\text{carb}}$ values and REE + Y patterns for the Tangshan section have been discussed by Li *et al.*⁴⁰ in detail. The $\delta^{13}\text{C}_{\text{org}}$ values vary from -31.77 to -22.24 ‰ (n = 84), with four positive (DP1, LP1, LP2 and BP1) and four negative (ECN, LN1, LN2, and BN1) excursions on the profile (Fig. 2). The $\delta^{13}\text{C}_{\text{org}}$ values for the DY Formation in the late Ediacaran vary from -28.15 to -22.24 ‰ (DP1), and they are positively correlated with

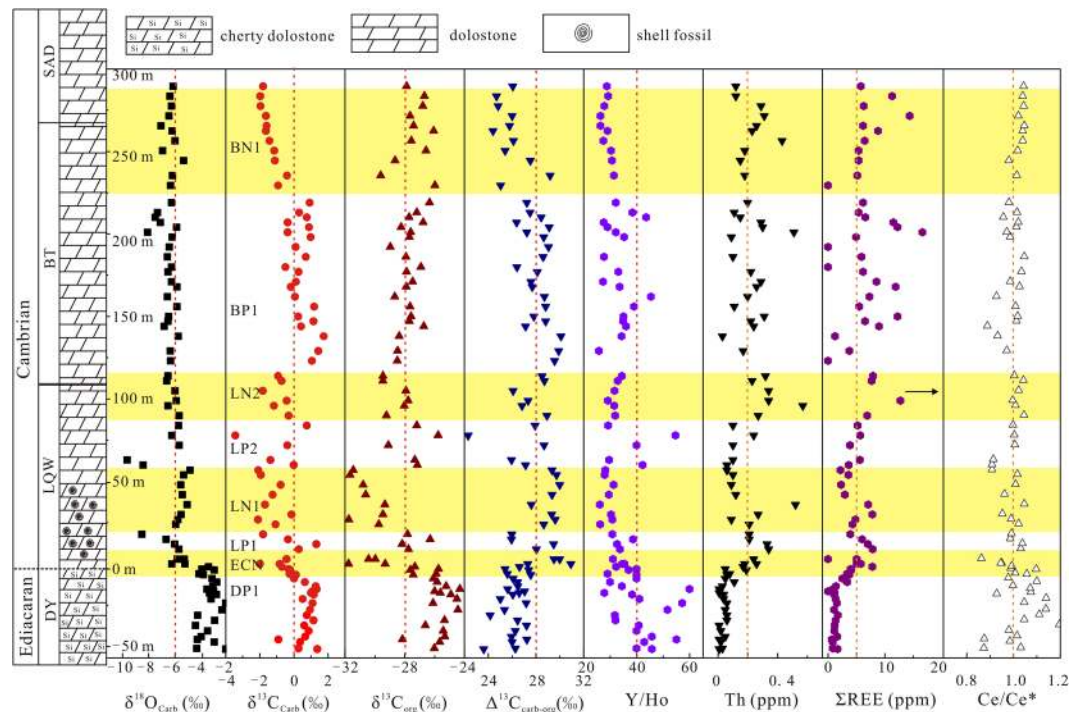


Figure 2. Lithological and geochemical profiles for dolostone from the Ediacaran to early Lower Cambrian strata in the Tangshan section.

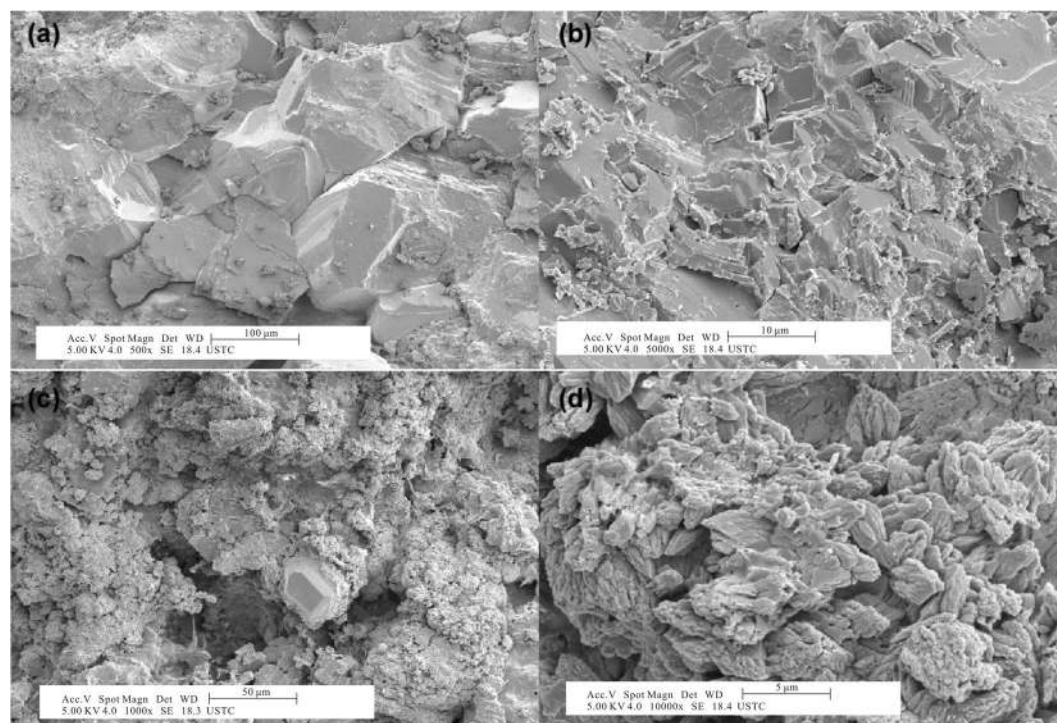


Figure 3. The SEM photograph of 12CH128 in the early Cambrian, (a) and (b) the compacted micrystalline dolomite. (b) and (c) the different forms of autogenetic calcite filled in the dolostone.

the $\delta^{13}\text{C}_{\text{carb}}$ values. The first negative $\delta^{13}\text{C}_{\text{org}}$ excursion (ECN) is coupled with BACE^{43–46} at the E-C transition (Fig. 3). An overlying positive $\delta^{13}\text{C}_{\text{org}}$ excursion (LP1) from -28.17 to -26.29‰ occurs in the lower part of the LQW Formation in the early Cambrian, followed by a negative $\delta^{13}\text{C}_{\text{org}}$ excursion (LN1) from -29.32 to -31.66‰ .

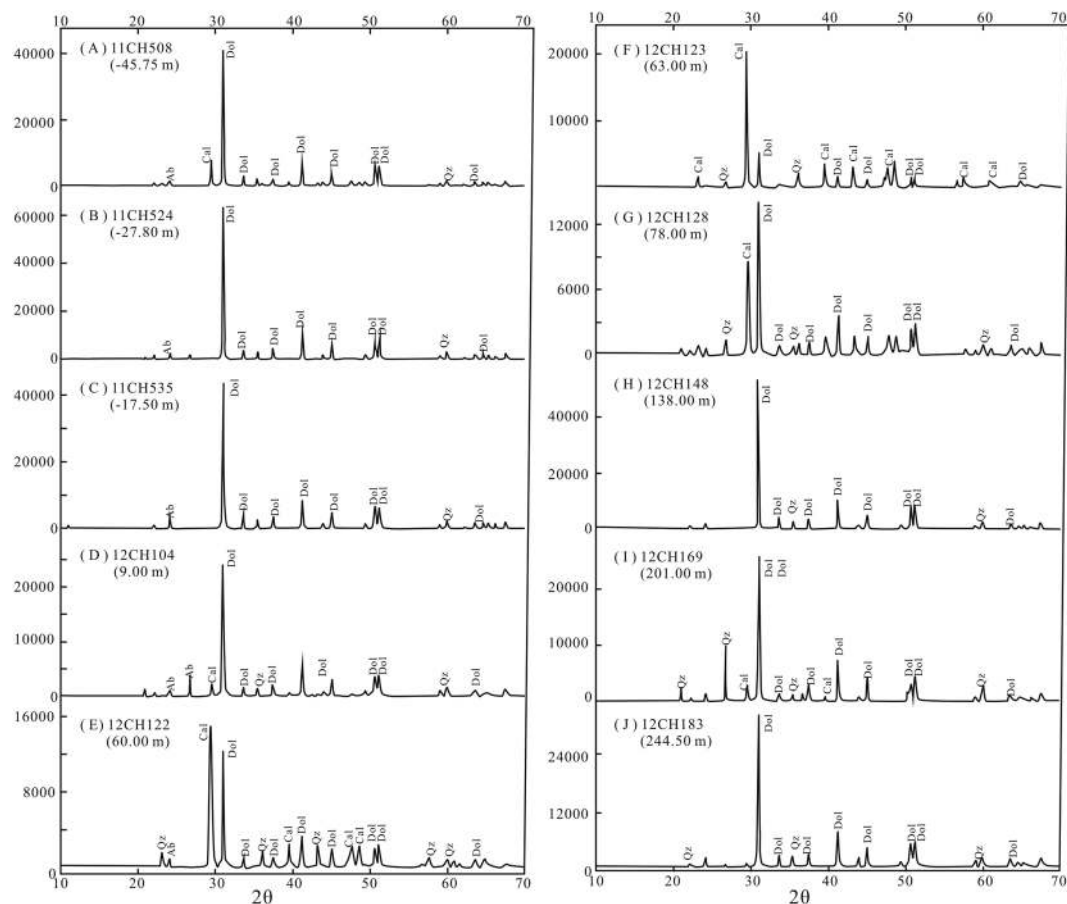


Figure 4. XRD results of the selected dolomite samples on the Tangshan section. The dolomite and calcite have characteristic peak below 30 and above 30, respectively. Dolomites 12CH122, 12CH123 and 12CH128 comprise much calcite crystal in the whole power.

A second positive $\delta^{13}\text{C}_{\text{org}}$ excursion (LP2) from -29.22 to -25.75‰ overlies LN1, followed by a third negative $\delta^{13}\text{C}_{\text{org}}$ excursion (LN2) from -29.46 to -28.53‰ at the boundary between the LQW and BT formations. Upwards, the $\delta^{13}\text{C}_{\text{org}}$ values vary with several $\delta^{13}\text{C}_{\text{carb}}$ fluctuations (Fig. 2), around -27.6 to -29.6‰ (including BP1 and BN1 for $\delta^{13}\text{C}_{\text{carb}}$) from the upper BT formation to the SAD Formation. The difference between the carbonate and organic carbon isotope compositions ($\Delta^{13}\text{C}_{\text{carb-org}} = \delta^{13}\text{C}_{\text{carb}} - \delta^{13}\text{C}_{\text{org}}$) varies between 22.31‰ and 30.93‰ , averaging 22.27‰ (Fig. 2). In particular, the $\Delta^{13}\text{C}_{\text{carb-org}}$ values in the early Cambrian LQW Formation (average 28.12‰) are abruptly higher than those in the late Ediacaran DY Formation (average 26.28‰) (Fig. 2).

Discussion

Preservation of primary geochemical features. Most samples from the Tangshan section are composed of dolomite with minor calcite. Dolomite grains show uniform equigranular and anhedral crystals with clear boundary (Fig. 3a,b, and Supplementary Table S1), implying insignificant alteration during post-depositional processes. Several samples were dedolomitized to calcite (Fig. 3c,d). In general, geochemical features such as carbon and oxygen isotope compositions and trace element concentrations are interpreted as primary geochemical signals related to the changes in seawater composition⁴⁰. However, post-depositional processes such as microbial remineralization and diagenetic alteration have a potential to alter the primary $\delta^{13}\text{C}_{\text{org}}$ values^{49,50}. In particular, the shallow marine carbonates on the Tangshan section could be periodically exposed during sea-level oscillations⁴⁰ and thus influenced by meteoric alteration⁵⁰. Therefore, it is essential to assess the preservation of primary $\delta^{13}\text{C}_{\text{org}}$ values. Although the preferential degradation of labile organic compounds can result in an elevation in $\delta^{13}\text{C}_{\text{org}}$ values of the residual organic carbon, it is impossible to generate a 4 to 5‰ $\delta^{13}\text{C}_{\text{org}}$ change in $\delta^{13}\text{C}_{\text{org}}$ values of the residual organic carbon during degradation⁵¹. In this regard, the $\delta^{13}\text{C}_{\text{org}}$ shift from -31.77 to -22.24‰ with a difference as large as 9‰ cannot be produced by the diagenetic alteration alone. In addition, the H/C ratios are higher than 0.2 (except several samples in the LQW and BT formations) and there is no correlations between H/C and $\delta^{13}\text{C}_{\text{org}}$ (Fig. 5, and Supplementary Table S1), indicating insignificant effect by the diagenetic alteration.

Carbon isotope chemostratigraphy. The E-C boundary is defined by the first appearance of small shelly fossils, *Treptichnus Pedum*^{52–54}. However, the relationship between the Ediacaran and Cambrian biotas is poorly known due to stratigraphic gaps, taphonomic bias, the restriction of metazoans to oxygenated habitats, and the difficulty in integrating commonly disparate bio- and chemostratigraphic data^{5,31,46,55}. The BACE, on the other hand,

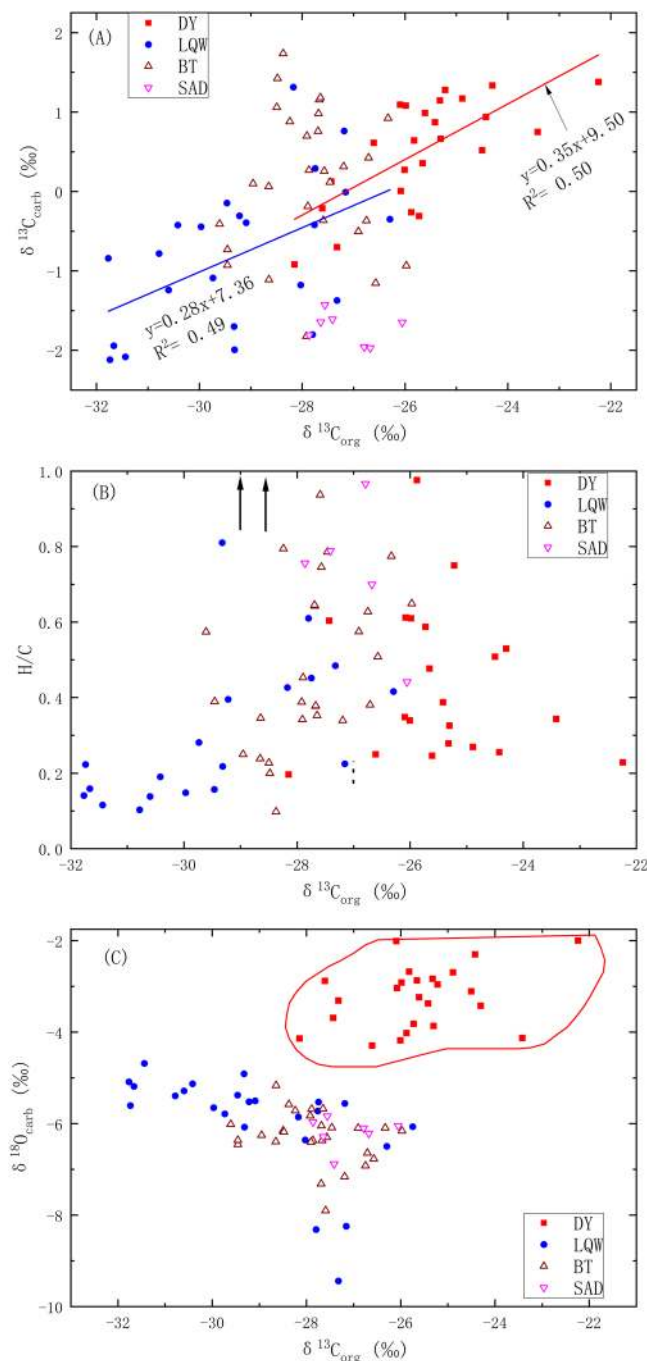


Figure 5. Correlations between $\delta^{13}\text{C}_{\text{org}}$ values and (A) $\delta^{13}\text{C}_{\text{carb}}$ values, (B) H/C ratios, (C) $\delta^{18}\text{O}_{\text{carb}}$ values for dolostone on the Tangshan section. The arrows in (B) represent the high H/C ratios for dolostone in the early Cambrian LQW formation.

was followed by the rapid appearance and diversification of bilaterian animals in the early Cambrian according to a combined study of lithology, fossils and geochemical data^{5,47}. Thus, it can be constrained and better correlated within the interval of characteristic Cambrian-type skeletal fossil distribution^{5,34,38,46,56,57}.

The E-C successions on the Tangshan section can be divided into eight $\delta^{13}\text{C}_{\text{carb}}$ intervals, from bottom to top named DP1, ECN, LP1, LN1, LP1, LN2, BP1 and BN1⁴⁰. The $\delta^{13}\text{C}_{\text{org}}$ values increase from -28.15 to -24.50‰ (DP1) in the Dengying Formation, which can be correlated in trend and magnitude with those of the Ganziping section in western Yunnan³⁴, the Jiuqunao, Hezi'ao and Jijiapo sections in Hubei⁵⁸. The DP1 are higher than the contemporaneous values for the Shantan section, the Songtao section⁴⁹, the Longbuzi section⁵⁹, the Yuantewan-Lijiatuo section⁴⁹ and the Ara Group⁶⁰.

The $\delta^{13}\text{C}_{\text{org}}$ excursions are coupled with the $\delta^{13}\text{C}_{\text{carb}}$ excursions in the late Ediacaran DY and the early Cambrian LQW formations (Fig. 5A). ECN, a negative $\delta^{13}\text{C}_{\text{org}}$ excursion of -4.4‰ from -27.32 to -31.77‰

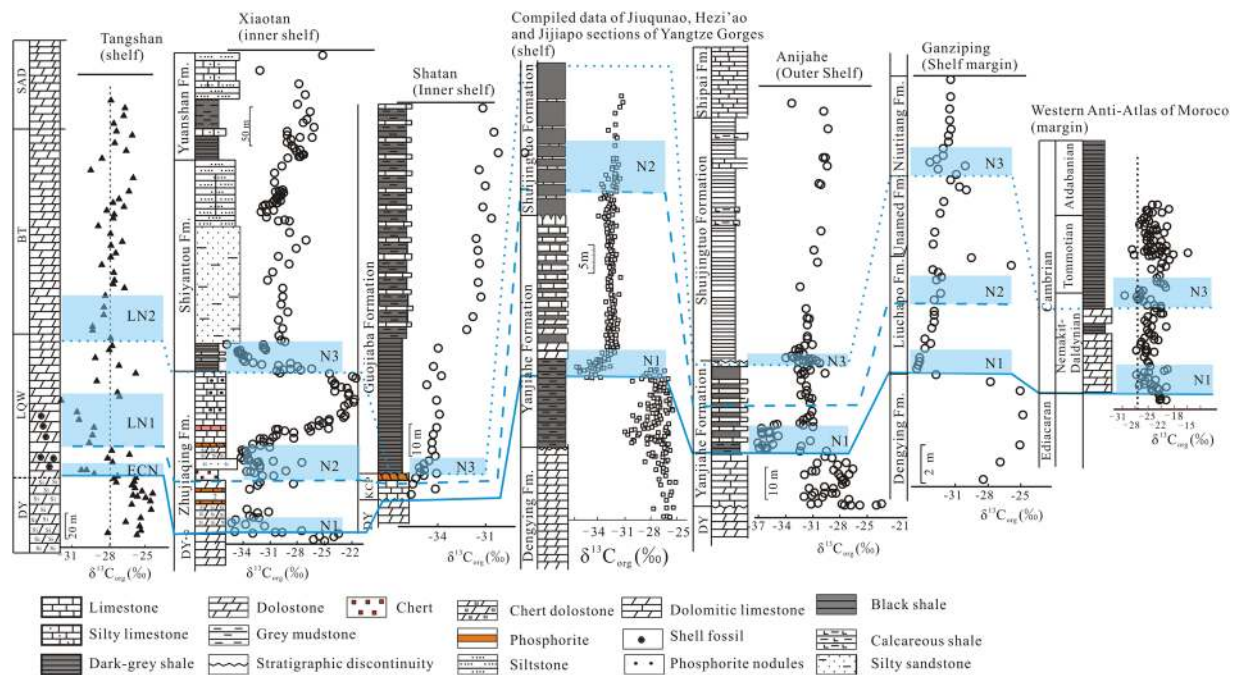


Figure 6. Variations in organic carbon isotope compositions across the Ediacaran-Cambrian transition on the Tangshan section and their stratigraphic correlations with those at Xiaotan⁵⁷, Shatan⁴⁹, Anjiahe³⁸, Ganziping³⁴, Yangtze Gorge⁵⁸ and the western Anti-Atlas margin of Morocco⁴⁶.

(Supplementary Table S1), can be identified at the E-C transition (Fig. 2), which can be correlated with the N1 at Xiaotan⁵⁷ and Shatan⁴⁹ of inner shelf, Anjiahe of outer shelf³⁸ and Ganziping of shelf margin³⁴. Corresponding shifts can also be found in the Jiuquao, Hezi'ao and Jijiapo sections on the Yangtze platform⁵⁶ (Fig. 6) and a shallow-water section in the western Anti-Atlas margin of Morocco⁴⁶. The worldwide ECN or N1 negative $\delta^{13}\text{C}_{\text{carb}}$ excursion, named the BACE^{5,45}, is consistent with the first appearance of small shelly fossils of *Anabarites trisulcatus* zone³³, which was calibrated as the beginning of Cambrian⁶¹.

Above the ECN (or BACE), a first large positive excursion in both $\delta^{13}\text{C}_{\text{carb}}$ and $\delta^{13}\text{C}_{\text{org}}$ (LP1) occurred (Fig. 5), followed by a second negative excursion in both $\delta^{13}\text{C}_{\text{carb}}$ and $\delta^{13}\text{C}_{\text{org}}$ (LN1). The ECN and LN1 can be correlated with the shallow-water carbonates from the other sections on the Yangtze platform (Fig. 6), but they may be lost on some sections due to the unconformity and stratigraphic condensation in shallow-water settings^{37,62}. The $\delta^{13}\text{C}_{\text{carb}}$ excursion in LN1 can be correlated with Cycle III on the Dovortsy section in Siberia⁶³, N2 on the Jiuquao section in Yichang⁵⁸ and the Anjiahe section in Yangtze Gorge³⁸, N2i on the Xiaotan section in Yunnan⁶⁴ and N2 on the Jiuquao, Hezi'ao and Jijiapo sections⁵⁸. Upwards, the second positive $\delta^{13}\text{C}_{\text{carb}}$ and $\delta^{13}\text{C}_{\text{org}}$ excursions (LP2) occurred and were overlain by the third negative $\delta^{13}\text{C}_{\text{carb}}$ and $\delta^{13}\text{C}_{\text{org}}$ excursions (LN2), which can be correlated with N3 on the Anjiahe section³⁷, C4⁵⁷ or N3 on the Xiaotan section³⁷, N3 on the Shatan⁴⁹, Daotuo³⁷, Longbizui³⁴ and Yuanwutan sections⁴⁹. In the present study, the three negative $\delta^{13}\text{C}_{\text{carb}}$ and $\delta^{13}\text{C}_{\text{org}}$ excursions (ECN, LN1 and LN2) are identified in the early Cambrian (Fig. 6). It should be noted that there is also a small negative $\delta^{13}\text{C}_{\text{carb}}$ excursion in the SAD Formation, but the $\delta^{13}\text{C}_{\text{org}}$ values are relatively stable (Fig. 2).

In addition, the $\delta^{13}\text{C}_{\text{org}}$ values largely vary between the different sections because C_{org} can be dominated by local influences associated with the mechanism and rate of carbon fixation, the degree of remineralization, terrestrial organic influx, and trophic structure³⁸. Existing $\delta^{13}\text{C}_{\text{org}}$ values from the earliest Cambrian in South China show a large variation from -31 to -37‰ (Fig. 6)^{34,38,49,57,58}.

The $\Delta^{13}\text{C}_{\text{carb-org}}$ between carbonate and organic matter. The $\delta^{13}\text{C}_{\text{carb}}$ and $\delta^{13}\text{C}_{\text{org}}$ values are coupled in the late Ediacaran DY Formation and the early Cambrian LQW Formation, but decoupled in the BT and SAD formations (Fig. 5A). In particular, the $\Delta^{13}\text{C}_{\text{carb-org}}$ values in the early Cambrian LQW Formation (average 28.12‰) are considerably higher than those in the late Ediacaran DY Formation (average 26.28‰) (Fig. 7), which also occurs on the other contemporary successions although the absolute $\Delta^{13}\text{C}_{\text{carb-org}}$ values vary with depositional settings (Fig. 7).

The evidence that the evolution of oxygenic photosynthesis had occurred by ~ 2.78 Ga is provided by the presence of 2- α methylhapanes from O_2 -producing cyanobacteria⁶⁵ and sterols from O_2 -requiring eukaryotes⁶⁶. Shortly before the Neoproterozoic glaciations, a significant diversification of eukaryotes occurred⁶⁷. In the narrow time interval between the Sturtian and Marinoan glaciations, the steroid diversity and marine planktonic algae had a rapid rise⁶⁸. The rise of algae would create nutrient, energy and photosynthesis, driving ecosystems towards larger and increasing complex organism⁶⁸ and huge environmental changes^{15,17,20}. Cultures show that the $\Delta^{13}\text{C}_{\text{carb-org}}$ values of marine algae are controlled by the environmental factors, such as temperature, growth rate, pH, CO_2 and O_2 concentration⁶⁹. It was concluded that the $\Delta^{13}\text{C}_{\text{carb-org}}$ values between CO_2 and cells are

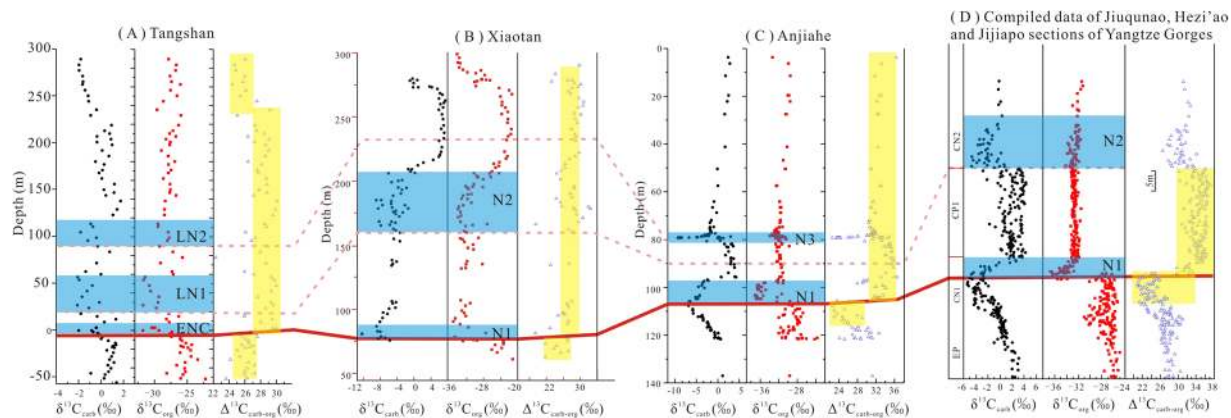


Figure 7. Plot of abrupt change in $\Delta^{13}\text{C}_{\text{carb-org}}$ values for the Tangshan section (this study), the Xiaotan section^{57,64}, the Anjiahe section³⁸ and the compiled data for Jiuqunao, Hezi'ao and Jijiapo sections at the Ediacaran-Cambrian boundary (the solid red line). The yellow areas indicate the variation of $\Delta^{13}\text{C}_{\text{carb-org}}$ values, and the blue areas are the correlation between $\delta^{13}\text{C}_{\text{org}}$ values in Fig. 6.

constant ($\sim 19\text{‰}$) from $10\text{ }^{\circ}\text{C}$ to $30\text{ }^{\circ}\text{C}$ ⁷⁰. Seawater temperatures were proposed to be lower than $34\text{ }^{\circ}\text{C}$ during the Cambrian^{71,72}. In this regard, the temperature effect on $\Delta^{13}\text{C}_{\text{carb-org}}$ values between CO_2 and cells can be negligible during the E-C transition. It is shown that a 2.7‰ change in carbon isotope fractionation can be associated with 0.1 shift in pH values⁶⁹, which is dependent upon P_{CO_2} and the influx of alkalinity. However, the $[\text{CO}_3]^{2-}$ concentrations are relatively stable in the early Cambrian²⁹. Therefore, the effect of pH variation on $\Delta^{13}\text{C}_{\text{carb-org}}$ values may not be important during the E-C transition.

Different photosynthesis species may be a factor related to $^{13}\text{C}/^{12}\text{C}$ fractionation, which may result from differences in growth rates and/or particulate organic carbon production³. Several experiments have indicated that the carbon isotope fractionation in algae or plants is primarily driven by the enzyme ribulose-1,5-bisphosphate Carboxylase/Oxygenase (RubisCO)⁷³, which is responsible for the fixation of CO_2 into organic compounds. The carbon fractionation between marine species and the partial pressure of atmospheric carbon dioxide ($p\text{CO}_2$) is clearly CO_2 -dependent, with higher $p\text{CO}_2$ leading to higher carbon isotope fractionation, which have been tested by dinoflagellate species³ and coccolithophorid with different growth rates⁴. Intrinsic carbon isotope fractionations associated with RubisCO have been estimated to be $\sim 22\text{‰}$ to 30‰ ⁷⁴. It has been shown that the $\delta^{13}\text{C}$ values of $p\text{CO}_2$ are associated with the carbon isotope composition of carbonate⁷⁵. The atmospheric concentration of CO_2 gas is kept near the Henry's Law equilibrium with surface seawater $[\text{HCO}_3]^-$ through gas exchange during turbulent mixing⁷⁵. Considering the limited variations in the pH, temperature and atmospheric pressure during the E-C transition^{29,71,72}, the equilibrium constant of carbon isotope exchange between gaseous and dissolved CO_2 varies in a small range^{76,77}. Thus, the limited carbon isotope fractionation between the atmospheric CO_2 and the marine dissolved inorganic carbon can be expected. The ^{13}C -discrimination between carboxylating reactions (RubisCO) and atmospheric CO_2 would likely be the reason for the abrupt changes in $\Delta^{13}\text{C}_{\text{carb-org}}$ during the E-C transition. However, the enhanced chemical weathering rate from the late Ediacaran DY Formation to the early Cambrian LQW Formation would cause a sudden CO_2 drawdown and cooling, which is recorded by the CIA index^{30,37,78,79}. It has been proven that the decrease of $p\text{CO}_2$ would have induced a decrease in the $\Delta^{13}\text{C}_{\text{carb-org}}$ values^{3,4}. In this way, the widespread and abrupt increase in $\Delta^{13}\text{C}_{\text{carb-org}}$ values during the E-C transition would not result from the variation in $p\text{CO}_2$ (Fig. 7).

The lowered $\delta^{13}\text{C}_{\text{org}}$ value can also be induced by the methanogenesis⁸⁰ and the elevated $\Delta^{13}\text{C}_{\text{carb-org}}$ excursion could be caused by the methanotrophic biomass⁸¹. However, the anaerobic carbon monoxide dehydrogenases (CODH) occur under strongly anoxic conditions⁸². In addition, the least oxygenation of surface seawater^{5,13-17} and the model calculations⁸³ indicate the sulfate concentrations during the early Cambrian were relatively high, which would reduce the role of methanogenesis. Thus, this possibility can safely be ruled out.

After the other environmental factors have been fully excluded, the best explanation for the abrupt increase in $\Delta^{13}\text{C}_{\text{carb-org}}$ values during the E-C transition is a rise in atmospheric O_2 . The dependence of biological carbon isotope fractionation on the partial pressure of atmospheric oxygen ($p\text{O}_2$) has been demonstrated in laboratory experiments with vascular land plants, bryophytes, and marine phytoplankton⁸⁴⁻⁸⁶. Increased carbon isotopic discrimination for light isotopes (^{12}C) is observed at increasing O_2 levels because atmospheric CO_2 levels rise within the plant of plankton cell as photorespiration begin to outpace photosynthesis, which in turn increases the carbon isotope fractionation during growth⁸⁵. In this way, the $p\text{O}_2$ increase can be expected by the increase of $\Delta^{13}\text{C}_{\text{carb-org}}$ values though the absolute values of $p\text{O}_2$ are notoriously difficult to track⁸⁷. Beerling *et al.*⁸⁵ have modeled the atmospheric O_2 dependence of the carbon isotope fractionation between fossil organic matter and CO_2 (equation 4 in their paper), which was modified by Saltzman, *et al.*⁸⁸ as:

$$\Delta^{13}\text{C}_{\text{meas}} = \Delta^{13}\text{C}_{\text{initial}} + J * \left[\frac{M_{\text{O}_2}}{38} \right] - 1 \quad (1)$$

where $\Delta^{13}\text{C}_{\text{meas}}$ is the measured value for the difference between $\delta^{13}\text{C}_{\text{carb}}$ and $\delta^{13}\text{C}_{\text{org}}$, and $\Delta^{13}\text{C}_{\text{initial}}$ is an estimate of the baseline value. In the present study, the average $\Delta^{13}\text{C}_{\text{carb-org}}$ value of 26.08‰ for the late Ediacaran DY

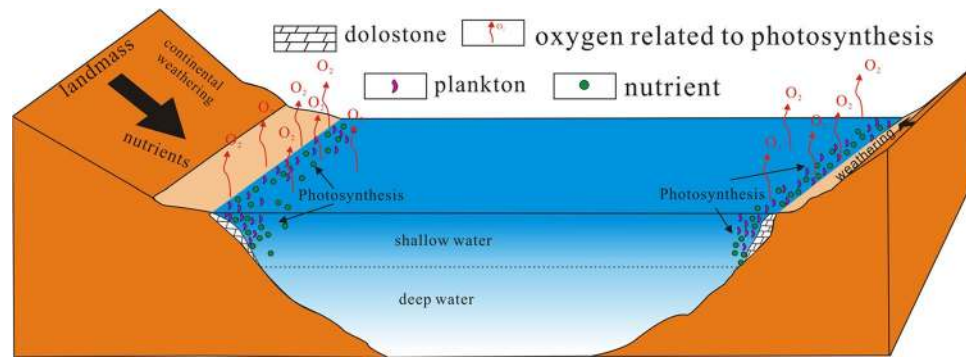


Figure 8. A conceptual model for the emergence of huge landmass and enhanced weathering, which results in the global scattering of nutrients into the seawater through river drainage and wind. This model coincide with the rise of atmospheric pO_2 due to the photosynthesis in the shallow seawater during Ediacaran-Cambrian transition.

formation is taken as the $\Delta^{13}C_{\text{initial}}$ value and the average $\Delta^{13}C_{\text{carb-org}}$ values of 28.07‰ for the early Cambrian LQW and BT formations are taken as the $\Delta^{13}C_{\text{meas}}$ value. A value of $J = 5$ is selected in the calculation based on the best fit to both the experimental data for isotopic discrimination in modern marine phytoplankton and the results of isotope mass balance model⁸⁸. Then, the abrupt increase in the $\Delta^{13}C_{\text{carb-org}}$ values of approximately +2‰ (Fig. 7) indicates that the mass of oxygen in the atmosphere was doubled in the early Cambrian^{85,88}. Although oxygen levels during the Late Neoproterozoic are difficult to constrain, it has been proposed that the oxygen levels are higher than 8% to 15% PAL near the end of the Neoproterozoic⁸⁹. In this regard, the pO_2 of early Cambrian would be at least 16 to 30% PAL, which is consistent with 10% to 40% PAL estimated for the Cambrian⁸⁷. The decrease of $\Delta^{13}C_{\text{carb-org}}$ values in the SAD Formation, equivalent to the middle Tommotian (Fig. 6), could be generated by another shift in pO_2 or pCO_2 ^{84,85,90} or the occurrence of new photosynthetic species⁹¹.

Continental trace element influx. During the E-C transition, a number of continental blocks were converged toward a large and complex continent, Gondwana^{27,92,93}. In general, this supercontinent is considered as an assembly of four major continental blocks along three collisional orogens²⁷. The convergent plate boundaries along the Gondwana-forming sutures could have served as effective sources for nutrient delivery⁹⁴. An unconformity was formed globally^{62,95}, followed by a worldwide transgression in the early Cambrian³⁶, which would expand the area of shallow epicontinental seas, leading to an increased accommodation space and a sustained flux of continental weathered products to the seawater (Fig. 8). This unconformity is recorded by shallow-water marine carbonates directly overlying on the continental crystalline basement, or basin/slope organic-rich shales/chert unconformably overlying the Ediacaran carbonate shelf at the Shatan and Anjiahe sections, but it is not recorded by those in deep-water sequences on the Longbizui and Yanwutan sections^{34,37,49,58,96}. The geochemical features, such as $\delta^{18}O_{\text{carb}}$ values, REE + Y patterns, water-insoluble element concentrations and Y/Ho ratios, suggest that the dolostones of the late Ediacaran DY Formation were deposited from normal seawater^{97,98}, but those of the early Cambrian LQW Formation were influenced by a large amount of continental weathered materials, which is consistent with a rapid rise in Sr isotope ratios^{99–102}. A number of elements, such as Be, Al, Sc, Co, Ga, Cs, REE, Hf and Th, are water-insoluble during chemical weathering given that they are concentrated in refractory minerals or strongly absorbed by clays¹⁰³. After intensive weathering, these elements were enriched in weathered products, which would be concentrated in the impure freshwater, in river, stream and lake¹⁰⁴, and ultimately into the seawater. In this way, the element concentrations and patterns of near-shore seawater would be altered by even a minor amount of terrigenous materials because the element compositions of terrigenous materials are quite different from that of seawater^{104,105}. The weathered products, including a widespread nutrient supply, such as P, K, Fe, Ca, Mg and others¹⁰⁶, could be transported to the shallow seawater via aeolian and fluvial systems across the global. Especially, the weathering flux of P into the seawater would increase, which could have promoted the activity of photosynthesis, leading a rise in atmospheric O_2 ^{28,107}.

Implications for coincidence in continental weathering and oxygen rise. The early Cambrian witnessed the explosive radiation of animals^{5,22,56}. Complex life requires two critical ingredients: nutrient and oxygen. Geological and geochemical studies indicate a constant increase of the oxygen level and a contraction of anoxic seawater during the E-C transition^{5,13–18}. It is hypothesized that the oxygenation was triggered through increased weathering fluxes^{21,28}, leading to an increase in oceanic primary production and organic carbon burial^{128,30,108}. The species engaging in ecosystem engineering might also be responsible for the oxygenation^{109,110}.

The emergence of huge landmass and the enhanced weathering of continental crust would transfer global scattering nutrients into the seawater through wind and river drainage in the early Cambrian (Fig. 8), which is indicated by the decrease of Y/Ho ratios and the increase of Th, V, Sc and REE concentrations (Fig. 2 and Supplementary Fig. S1). Although it is difficult to accurately constrain the proportions of fresh water in the surface seawater, the relative proportions of freshwater can be obtained on the basis of the $\delta^{18}O_{\text{carb}}$ values, the water-insoluble element concentrations, Y/Ho ratios (Supplementary Fig. S3). The mixing lines between $\delta^{18}O_{\text{carb}}$ values and Y/Ho ratios represent a result of mixing two end-members between seawater and freshwater, where the freshwater contains the terrigenous material from the chemical weathering into the seawater (Supplementary Fig. S3).

The chemical weathering not only serves as a negative feedback for CO₂, but also provides the nutrients for feeding of the primary producers. A stable supply of essential nutrients would also exert a significant control on the evolution of myriad life forms²⁷. Nutrients, such as P, Ca, Fe, Na⁺, K⁺ and Mo, are predominantly enriched in crustal rocks, such as granitoids and andesite²⁷. These elements are critically important to build the 'hard parts' (bones, shells, teeth), whereas some of the other nutrients are essential for cell metabolism¹⁰⁶. Enormous nutrient into the seawater would especially feed the planktons in the sea surface¹⁰⁶, leading to an accelerated burst of photosynthesis^{67,111}, which may be the Earth's only major source of molecular oxygen, an oxygen source strong enough to sustain a major atmospheric oxygen increase¹¹². The atmospheric O₂ could reach up to 16 to 30% PAL based on the abrupt increase of $\Delta^{13}\text{C}_{\text{carb-org}}$ values during the E-C transition (Fig. 7). Although anoxic seawaters may still have existed widely in the early Cambrian^{87,113}, evidence from sedimentary Mo concentrations^{5,13,14} and isotopes¹⁵, U isotopes^{16,17} and its rare earth element concentrations¹⁸ indicate strong oxygenation of the deep seawater¹⁵, consistent with the rise of atmospheric oxygen concentrations^{113–115} and the appearance of filter-feeding sponges^{30,31,110}.

Although the timing and magnitude of atmospheric O₂ accumulation are difficult to be accurately constrained, it is supposed to be regulated by erosion and deposition related to tectonic processes^{30,116}. An imbalance between the oxygen production and consumption would result in a gradual rise in the oxygen accumulation^{30,109,116}. The high *p*O₂ is necessary to keep the reaction at the seawater-atmosphere interface in order to produce collagen that paste plural cells together. However, even if the *p*O₂ is high enough, metazoans cannot be synthesized if the nutrient elements that make up the metazoans were not supplied¹⁰⁶. In this regard, the simultaneously enhanced weathering input would provide necessary nutrients for biological evolution. Therefore, the increasing amount of landmass, the enhancement of chemical weathering on the continental crust, the supply of a large amount of nutrients into the shelf and high oxygen level in the atmosphere all coincide in time for promoting the birth of large multi-cellular animals.

Conclusions

The Ediacaran-Cambrian (E-C) transition is a period with substantial biospheric, environmental, and tectonic changes. The $\delta^{13}\text{C}_{\text{org}}$ profile on the Tangshan section in South China records three negative excursions during the early Cambrian, which can be compared with those of the other sections in the world. The abrupt increase in $\Delta^{13}\text{C}_{\text{carb-org}}$ values indicates a rise of atmospheric oxygen concentrations at the E-C boundary. Although there are several $\delta^{13}\text{C}_{\text{carb}}$ and $\delta^{13}\text{C}_{\text{org}}$ excursions in the early Cambrian, the atmospheric O₂ retained high during the deposition of the LQW and BT formations. Geochemical proxies, such as REE + Y patterns, water-insoluble element concentrations and Y/Ho ratios, indicate that an enhanced weathering of the continental crust occurred from the late Ediacaran DY Formation to the early Cambrian LQW Formation during the E-C transition. The enhancement of continental weathering delivers nutrients to the seawater for primary producers, which would accelerate photosynthesis and promote the rise of atmospheric *p*O₂. The enhanced weathering along with the rise of atmospheric oxygen, may have boosted the emergence of complex life in the early Cambrian.

Methods

Some samples and the method of trace element concentrations have been described in Li *et al.*⁴⁰. The methods of this study are as following.

XRD. The Mg/Ca ratios of all samples were analyzed by Li *et al.*⁴⁰. Only several sample powders with special Mg/Ca ratios were measured in the present study by X-ray diffraction (XRD). The XRD analysis was performed at University of Science and Technology of China (USTC) in Hefei using a TTR-III diffractometer (operating at 40 kV, 200 mA) equipped with a fixed graphite monochromator and a Cu target tube in the 2 θ with a steep size of 0.02 degree. Meanwhile, the microstructure of the carbonate was observed by the scanning electron microscope (SEM) at USTC.

Oxygen and carbon isotopes. The methods for the analyses of carbonate C and O isotopes ($\delta^{13}\text{C}_{\text{carb}}$ and $\delta^{18}\text{O}_{\text{carb}}$) were presented in Li *et al.*⁴⁰. The organic carbon isotope compositions ($\delta^{13}\text{C}_{\text{org}}$) were measured on 84 samples. The 50% (v/v) guarantee reagent hydrochloric acid had been used at 60 °C for 24 h to remove the all carbonate components in whole-rock powders, and the undissolved part was washed by ultra-pure water and extracted for three times to achieve neutral solution conditions¹⁹. The undissolved part of the carbonate were dried at 70 °C and weighed, and then they were analyzed to get the TC, TH and TN of the residue by the Elementar vario EL cube at USTC. The analytical precisions of TC, TH and TN are better than $\pm 0.3\%$. The organic carbon isotopes of the residues were analyzed via online EA-1112 link to Finigan Delta-Plus XL at State Key Laboratory of Organic Geochemistry in Guangzhou Institute of Geochemistry, Chinese Academy of Sciences (CAS), Guangzhou. The results are calibrated from the standard carbon black $\delta^{13}\text{C}_{\text{PDB}} = -36.91\%$ and given in the standard delta notation as per mil difference to the Vienna PDB standard (VPDB). Reproducibility was generally better than $\pm 0.5\%$.

References

1. Anbar, A. D. & Knoll, A. H. Proterozoic ocean chemistry and evolution: a bioinorganic bridge? *Science* **297**, 1137–1142 (2002).
2. Berner, R. A., VandenBrooks, J. M. & Ward, P. D. Oxygen and Evolution. *Science* **316**, 557–558 (2007).
3. Hoins, M. *et al.* Stable carbon isotope fractionation of organic cyst-forming dinoflagellates: Evaluating the potential for a CO₂ proxy. *Geochim. Cosmochim. Acta* **160**, 267–276 (2015).
4. Rost, B., Zondervan, I. & Riebesell, U. Light-dependent carbon isotope fractionation in the coccolithophorid *Emiliania huxleyi*. *Limnol. Oceanogr.* **47**, 120–128 (2002).
5. Zhu, M., Zhuravlev, A. Y., Wood, R. A., Zhao, F. & Sukhov, S. S. A deep root for the Cambrian explosion: Implications of new bio- and chemostratigraphy from the Siberian Platform. *Geology* **45**, 459–462 (2017).

6. Canfield, D. E. *et al.* Ferruginous Conditions Dominated Later Neoproterozoic Deep-Water Chemistry. *Science* **321**, 949–952 (2008).
7. Kimura, H. & Watanabe, Y. Oceanic anoxia at the Precambrian–Cambrian boundary. *Geology* **29**, 995–998 (2001).
8. Liu, K., Feng, Q., Shen, J., Khan, M. & Planavsky, N. J. Increased productivity as a primary driver of marine anoxia in the Lower Cambrian. *Palaeogeogr. Palaeoclimatol. Palaeoecol.* **491**, 1–9 (2018).
9. Jin, C. *et al.* A highly redox-heterogeneous ocean in South China during the early Cambrian (~529–514 Ma): Implications for biota-environment co-evolution. *Earth Planet. Sci. Lett.* **441**, 38–51 (2016).
10. Guo, Q. *et al.* Trace element chemostratigraphy of two Ediacaran–Cambrian successions in South China: Implications for organosedimentary metal enrichment and silicification in the Early Cambrian. *Palaeogeogr. Palaeoclimatol. Palaeoecol.* **254**, 194–216 (2007).
11. Wei, G.-Y. *et al.* Marine redox fluctuation as a potential trigger for the Cambrian explosion. *Geology* **46**, 587–590 (2018).
12. Wen, H., Fan, H., Zhang, Y., Cloquet, C. & Carignan, J. Reconstruction of early Cambrian ocean chemistry from Mo isotopes. *Geochim. Cosmochim. Acta* **164**, 1–16 (2015).
13. Scott, C. *et al.* Tracing the stepwise oxygenation of the Proterozoic ocean. *Nature* **452**, 456–459 (2008).
14. Chang, C. *et al.* Characterization of trace elements and carbon isotopes across the Ediacaran–Cambrian boundary in Anhui Province, South China: Implications for stratigraphy and paleoenvironment reconstruction. *J. Asian Earth Sci.* (2016).
15. Chen, X. *et al.* Rise to modern levels of ocean oxygenation coincided with the Cambrian radiation of animals. *Nat Commun* **6** (2015).
16. Tostevin, R. *et al.* Uranium isotope evidence for an expansion of anoxia in terminal Ediacaran oceans. *Earth Planet. Sci. Lett.* **506**, 104–112 (2019).
17. Kendall, B. *et al.* Uranium and molybdenum isotope evidence for an episode of widespread ocean oxygenation during the late Ediacaran Period. *Geochim. Cosmochim. Acta* **156**, 173–193 (2015).
18. Ling, H.-F. *et al.* Cerium anomaly variations in Ediacaran–earliest Cambrian carbonates from the Yangtze Gorges area, South China: Implications for oxygenation of coeval shallow seawater. *Precamb. Res.* **225**, 110–127 (2013).
19. Krause, A. J. *et al.* Stepwise oxygenation of the Paleozoic atmosphere. *Nature Communications* **9**, 4081 (2018).
20. Wallace, M. W. *et al.* Oxygenation history of the Neoproterozoic to early Phanerozoic and the rise of land plants. *Earth Planet. Sci. Lett.* **466**, 12–19 (2017).
21. Mills, B., Lenton, T. M. & Watson, A. J. Proterozoic oxygen rise linked to shifting balance between seafloor and terrestrial weathering. *Proceedings of the National Academy of Sciences of the United States of America* **111**, 9073–9078 (2014).
22. Erwin, D. H. *et al.* The Cambrian Conundrum: Early Divergence and Later Ecological Success in the Early History of Animals. *Science* **334**, 1091–1097 (2011).
23. Sperling, E. A. *et al.* Oxygen, ecology, and the Cambrian radiation of animals. *Proceedings of the National Academy of Sciences* **110**, 13446–13451 (2013).
24. Smith, M. P. & Harper, D. A. T. Causes of the Cambrian Explosion. *Science* **341**, 1355–1356 (2013).
25. Mills, D. B. *et al.* Oxygen requirements of the earliest animals. *Proceedings of the National Academy of Sciences* **111**, 4168–4172 (2014).
26. Mills, D. B. & Canfield, D. E. Oxygen and animal evolution: Did a rise of atmospheric oxygen “trigger” the origin of animals? *BioEssays* **36**, 1145–1155 (2014).
27. Santosh, M., Maruyama, S., Sawaki, Y. & Meert, J. G. The Cambrian Explosion: Plume-driven birth of the second ecosystem on Earth. *Gondwana Res.* **25**, 945–965 (2014).
28. Planavsky, N. J. *et al.* The evolution of the marine phosphate reservoir. *Nature* **467**, 1088 (2010).
29. Riding, R. & Liang, L. Seawater chemistry control of marine limestone accumulation over the past 550 million years. Vol. 37 (2005).
30. Lenton, T. M. & Watson, A. J. Biotic enhancement of weathering, atmospheric oxygen and carbon dioxide in the Neoproterozoic. *Geophys. Res. Lett.* **31** (2004).
31. Erwin, D. H. & Tweedt, S. Ecological drivers of the Ediacaran–Cambrian diversification of Metazoa. *Evol. Ecol.* **26**, 417–433 (2012).
32. Wang, J. & Li, Z. X. History of Neoproterozoic rift basins in South China: implications for Rodinia break-up. *Precamb. Res.* **122**, 141–158 (2003).
33. Maloof, A. *et al.* The earliest Cambrian record of animals and ocean geochemical change. *Bulletin of the Geological Society of America* **122**, 1731–1774 (2010).
34. Chen, D., Wang, J., Qing, H., Yan, D. & Li, R. Hydrothermal venting activities in the Early Cambrian, South China: Petrological, geochronological and stable isotopic constraints. *Chem. Geol.* **258**, 168–181 (2009).
35. Guo, Q., Deng, Y., Hippler, D., Franz, G. & Zhang, J. REE and trace element patterns from organic-rich rocks of the Ediacaran–Cambrian transitional interval. *Gondwana Res.* **36**, 94–106 (2016).
36. Steiner, M., Wallis, E., Erdtmann, B.-D., Zhao, Y. & Yang, R. Submarine-hydrothermal exhalative ore layers in black shales from South China and associated fossils — insights into a Lower Cambrian facies and bio-evolution. *Palaeogeogr. Palaeoclimatol. Palaeoecol.* **169**, 165–191 (2001).
37. Zhai, L., Wu, C., Ye, Y., Zhang, S. & Wang, Y. Fluctuations in chemical weathering on the Yangtze Block during the Ediacaran–Cambrian transition: Implications for paleoclimatic conditions and the marine carbon cycle. *Palaeogeogr. Palaeoclimatol. Palaeoecol.* **490**, 280–292 (2018).
38. Ishikawa, T. *et al.* Irreversible change of the oceanic carbon cycle in the earliest Cambrian: High-resolution organic and inorganic carbon chemostratigraphy in the Three Gorges area, South China. *Precamb. Res.* **225**, 190–208 (2013).
39. Sun, C. Diachronism of the bantang delitic dolomite in the chaohu lake area Anhui. *Regional Geology of China* **4**, 380–383 (Chinese with English Abstract) (1988).
40. Li, W.-P., Zheng, Y.-F. & Zhao, Y.-Y. Geochemical evidence from marine carbonate for enhanced terrigenous input into seawater during the Ediacaran–Cambrian transition in South China. *Precamb. Res.* **291**, 83–97 (2017).
41. Compston, W., Zhang, Z., Cooper, J. A., Ma, G. & Jenkins, R. J. F. Further SHRIMP geochronology on the early Cambrian of South China. *Am. J. Sci.* **308**, 399–420 (2008).
42. Jiang, S.-Y. *et al.* Early Cambrian ocean anoxia in South China. *Nature* **459**, E5 (2009).
43. Zhu, M.-Y., Babcock, L. E. & Peng, S.-C. Advances in Cambrian stratigraphy and paleontology: Integrating correlation techniques. *paleobiology, taphonomy and paleoenvironmental reconstruction. Palaeoworld* **15**, 217–222 (2006).
44. Landing, E., Peng, S., Babcock, L., Geyer, G. & Moczydlowska-Vidal, M. Global standard names for the lowermost Cambrian series and stage. *Episodes* **30**, 287–289 (2007).
45. Zhu, M. Y., Strauss, H. & Shields, G. A. From snowball earth to the Cambrian bioradiation: Calibration of Ediacaran–Cambrian earth history in South China. *Palaeogeogr. Palaeoclimatol. Palaeoecol.* **254**, 1–6 (2007).
46. Maloof, A. C. *et al.* Constraints on early Cambrian carbon cycling from the duration of the Nemakit–Daldynian–Tommotian boundary 13C shift, Morocco. *Geology* **38**, 623–626 (2010).
47. Amthor, J. E. *et al.* Extinction of Cloudina and Namacalathus at the Precambrian–Cambrian boundary in Oman. *Geology* **31**, 431–434 (2003).
48. Bowring, S. *et al.* Geochronologic constraints on the chronostratigraphic framework of the Neoproterozoic Huqf Supergroup of Oman. *Am. J. Sci.* **307**, 1097–1145 (2007).
49. Guo, Q. *et al.* Carbon isotopic evolution of the terminal Neoproterozoic and early Cambrian: Evidence from the Yangtze Platform, South China. *Palaeogeogr. Palaeoclimatol. Palaeoecol.* **254**, 140–157 (2007).
50. Oehlert, A. M. & Swart, P. K. Interpreting carbonate and organic carbon isotope covariance in the sedimentary record. *Nature Communications* **5**, 4672 (2014).

51. Lehmann, M. F., Bernasconi, S. M., Barbieri, A. & McKenzie, J. A. Preservation of organic matter and alteration of its carbon and nitrogen isotope composition during simulated and *in situ* early sedimentary diagenesis. *Geochim. Cosmochim. Acta* **66**, 3573–3584 (2002).
52. Landing, E. Precambrian–Cambrian boundary global stratotype ratified and a new perspective of Cambrian time. *Geology* **22**, 179–182 (1994).
53. Brasier, M., Cowie, J. & Taylor, M. Decision on the Precambrian–Cambrian boundary stratotype. Vol. 17 (1994).
54. Buatois, L. A. *Treptichnus pedum* and the Ediacaran–Cambrian boundary: significance and caveats. *Geol. Mag.* **155**, 174–180 (2018).
55. Schiffbauer, J. D. Research focus: The age of tubes: A window into biological transition at the Precambrian–Cambrian boundary. *Geology* **44**, 975–976 (2016).
56. Smith, E. F. *et al.* The end of the Ediacaran: Two new exceptionally preserved body fossil assemblages from Mount Dunfee, Nevada, USA. *Geology* **44**, 911–914 (2016).
57. Cremonese, L. *et al.* Marine biogeochemical cycling during the early Cambrian constrained by a nitrogen and organic carbon isotope study of the Xiaotan section. *South China. Precamb. Res.* **225**, 148–165 (2013).
58. Jiang, G. *et al.* The origin of decoupled carbonate and organic carbon isotope signatures in the early Cambrian (ca. 542–520Ma) Yangtze platform. *Earth Planet. Sci. Lett.* **317–318**, 96–110 (2012).
59. Wang, J., Chen, D., Yan, D., Wei, H. & Xiang, L. Evolution from an anoxic to oxic deep ocean during the Ediacaran–Cambrian transition and implications for bioturbation. *Chem. Geol.* **306–307**, 129–138 (2012).
60. Fike, D. A. *Carbon and Sulfur Isotopic Constraints on Ediacaran Biogeochemical Processes, Huqf Supergroup, Sultanate of Oman* ph.D. thesis, Cambridge, Massachusetts, (2007).
61. Kaufman, A. *et al.* Integrated chronostratigraphy of Proterozoic–Cambrian boundary beds in the western Anabar region, Northern Siberia. *Geol. Mag.* **133**, 509–533 (1996).
62. Peters, S. E. & Gaines, R. R. Formation of the ‘Great Unconformity’ as a trigger for the Cambrian explosion. *Nature* **484**, 363–366 (2012).
63. Magaritz, M., Kirschvink, J. L., Latham, A. J., Zhuravlev, A. Y. & Rozanov, A. Y. Precambrian/Cambrian boundary problem: Carbon isotope correlations for Vendian and Tommotian time between Siberia and Morocco. *Geology* **19**, 847–850 (1991).
64. Li, D. *et al.* Carbon and strontium isotope evolution of seawater across the Ediacaran–Cambrian transition: Evidence from the Xiaotan section, NE Yunnan, South China. *Precambrian Research* **225**, 128–147 (2013).
65. Brocks, J. J., Logan, G. A., Buick, R. & Summons, R. E. Archean molecular fossils and the early rise of eukaryotes. *Science* **285**, 1033–1036 (1999).
66. Summons, R. E., Jahnke, L. L., Hope, J. M. & Logan, G. A. 2-Methylhopanoids as biomarkers for cyanobacterial oxygenic photosynthesis. *Nature* **400**, 554–557 (1999).
67. Lenton, T. M., Boyle, R. A., Poulton, S. W., Shields-Zhou, G. A. & Butterfield, N. J. Co-evolution of eukaryotes and ocean oxygenation in the Neoproterozoic era. *Nature Geoscience* **7**, 257 (2014).
68. Brocks, J. J. *et al.* The rise of algae in Cryogenian oceans and the emergence of animals. *Nature* **548**, 578 (2017).
69. Hinga, K. R., Arthur, M. A., Pilson, M. E. Q. & Whitaker, D. Carbon isotope fractionation by marine phytoplankton in culture: The effects of CO₂ concentration, pH, temperature, and species. *Global Biogeochem. Cycles* **8**, 91–102 (1994).
70. Degens, E. T., Guillard, R. R. L., Sackett, W. M. & Hellebust, J. A. Metabolic fractionation of carbon isotopes in marine plankton; 1, Temperature and respiration experiments. *Deep-Sea Research and Oceanographic Abstracts* **15**, 1–9 (1968).
71. Jaffrés, J. B. D., Shields, G. A. & Wallmann, K. The oxygen isotope evolution of seawater: a critical review of a long-standing controversy and an improved geological water cycle model for the past 3.4 billion years. *Earth Sci. Rev.* **83**, 83–122 (2007).
72. Robert, F. & Chaussidon, M. A palaeotemperature curve for the Precambrian oceans based on silicon isotopes in cherts. *Nature* **443**, 920–921 (2006).
73. Roeske, C. A. & O’Leary, M. H. Carbon isotope effects on enzyme-catalyzed carboxylation of ribulose biphosphate. *Biochemistry* **23**, 6275–6284 (1984).
74. Scott, K. M. *et al.* Kinetic isotope effect and biochemical characterization of form IA RubisCO from the marine cyanobacterium *Prochlorococcus marinus* MIT9313. *Limnol. Oceanogr.* **52**, 2199–2204 (2007).
75. Ripperdan, E. L. In *Stable Isotope Geochemistry* Vol. 43 (eds Valley, J. W. & Cole, D. R.) 637–662 (Blackburg, Virginia, 2001).
76. Myrtilinen, A., Becker, V. & Barth, J. A. C. A review of methods used for equilibrium isotope fractionation investigations between dissolved inorganic carbon and CO₂. *Earth-Sci. Rev.* **115**, 192–199 (2012).
77. Szaran, J. Carbon isotope fractionation between dissolved and gaseous carbon dioxide. *Chem. Geol.* **150**, 331–337 (1998).
78. Donnadiu, Y., Goddérès, Y., Ramstein, G., Nédélec, A. & Meert, J. A. ‘snowball Earth’ climate triggered by continental break-up through changes in runoff. *Nature* **428**, 303 (2004).
79. Dessert, C., Dupré, B., Gaillardet, J., François, L. M. & Allègre, C. J. Basalt weathering laws and the impact of basalt weathering on the global carbon cycle. *Chem. Geol.* **202**, 257–273 (2003).
80. Qu, Y., Crne, A. E., Lepland, A. & van Zuilen, M. A. Methanotrophy in a Paleoproterozoic oil field ecosystem, Zaonega Formation, Karelia, Russia. *Geobiology* **10**, 467–478 (2012).
81. Zerkle, A. L., House, C. H. & Brantley, S. L. Biogeochemical signatures through time as inferred from whole microbial genomes. *Am. J. Sci.* **305**, 467–502 (2005).
82. Techtman, S., Colman, A., Lebedinsky, A., Sokolova, T. & Robb, F. Evidence for Horizontal Gene Transfer of Anaerobic Carbon Monoxide Dehydrogenases. *Frontiers in Microbiology* **3** (2012).
83. Schrag, D. P., Higgins, J. A., Macdonald, F. A. & Johnston, D. T. Authigenic Carbonate and the History of the Global Carbon Cycle. *Science* **339**, 540–543 (2013).
84. Berner, R. A. *et al.* Isotope Fractionation and Atmospheric Oxygen: Implications for Phanerozoic O₂ Evolution. *Science* **287**, 1630–1633 (2000).
85. Beerling, D. J. *et al.* Carbon isotope evidence implying high O₂/CO₂ ratios in the Permo–Carboniferous atmosphere. *Geochim. Cosmochim. Acta* **66**, 3757–3767 (2002).
86. Fletcher, B. J., Brentnall, S. J., Quick, W. P. & Beerling, D. J. BRYOCARB: A process-based model of thallose liverwort carbon isotope fractionation in response to CO₂, O₂, light and temperature. *Geochim. Cosmochim. Acta* **70**, 5676–5691 (2006).
87. Sperling, E. A. *et al.* Statistical analysis of iron geochemical data suggests limited late Proterozoic oxygenation. *Nature* **523**, 451 (2015).
88. Saltzman, M. R. *et al.* Pulse of atmospheric oxygen during the late Cambrian. *Proceedings of the National Academy of Sciences* (2011).
89. Canfield, D. E. The early history of atmospheric oxygen. *Annual Review of Earth and Planetary Sciences: homage to Robert M. Garrels* **33**, 1–36 (2005).
90. Kump, L. R. & Arthur, M. A. Interpreting carbon-isotope excursions: carbonates and organic matter. *Chem. Geol.* **161**, 181–198 (1999).
91. Zhang, X. *et al.* Triggers for the Cambrian explosion: Hypotheses and problems. *Gondwana Res.* **25**, 896–909 (2014).
92. Meert, J. G. & Lieberman, B. S. The Neoproterozoic assembly of Gondwana and its relationship to the Ediacaran–Cambrian radiation. *Gondwana Res.* **14**, 5–21 (2008).
93. Collins, A. S., Clark, C. & Plavsa, D. Peninsular India in Gondwana: The tectonothermal evolution of the Southern Granulite Terrain and its Gondwanan counterparts. *Gondwana Res.* **25**, 190–203 (2014).
94. Squire, R. J., Campbell, I. H., Allen, C. M. & Wilson, C. J. L. Did the Transgondwanan Supermountain trigger the explosive radiation of animals on Earth? *Earth Planet. Sci. Lett.* **250**, 116–133 (2006).

95. Keller, C. B. *et al.* Neoproterozoic glacial origin of the Great Unconformity. *Proceedings of the National Academy of Sciences* **116**, 1136–1145 (2019).
96. Ishikawa, T. *et al.* Carbon isotope chemostratigraphy of a Precambrian/Cambrian boundary section in the Three Gorge area, South China: Prominent global-scale isotope excursions just before the Cambrian Explosion. *Gondwana Research* **14**, 193–208 (2008).
97. Zhang, J. & Nozaki, Y. Rare earth elements and yttrium in seawater: ICP-MS determinations in the East Caroline, Coral Sea, and South Fiji basins of the western South Pacific Ocean. *Geochim. Cosmochim. Acta* **60**, 4631–4644 (1996).
98. Kamber, B. S. & Webb, G. E. The geochemistry of late Archaean microbial carbonate: implications for ocean chemistry and continental erosion history. *Geochim. Cosmochim. Acta* **65**, 2509–2525 (2001).
99. Cox, G. M. *et al.* Continental flood basalt weathering as a trigger for Neoproterozoic Snowball Earth. *Earth Planet. Sci. Lett.* **446**, 89–99 (2016).
100. van der Meer, D. G. *et al.* Reconstructing first-order changes in sea level during the Phanerozoic and Neoproterozoic using strontium isotopes. *Gondwana Res.* **44**, 22–34 (2017).
101. Shields, G. & Stille, P. Diagenetic constraints on the use of cerium anomalies as palaeoseawater redox proxies: An isotopic and REE study of Cambrian phosphorites. *Chem. Geol.* **175**, 29–48 (2001).
102. Melezhik, V. A., Gorokhov, I. M., Kuznetsov, A. B. & Fallick, A. E. Chemostratigraphy of Neoproterozoic carbonates: implications for 'bind dating'. *Terra Nova* **13**, 1–11 (2001).
103. Zhao, M.-Y. & Zheng, Y. F. Marine carbonate records of terrigenous input into Paleotethyan seawater: Geochemical constraints from Carboniferous limestones. *Geochim. Cosmochim. Acta* **141**, 508–531 (2014).
104. Lawrence, M. G., Greig, A., Collerson, K. D. & Kamber, B. S. Rare Earth Element and Yttrium Variability in South East Queensland Waterways. *Aquatic Geochemistry* **12**, 39–72 (2006).
105. Nothdurft, L. D., Webb, G. E. & Kamber, B. S. Rare earth element geochemistry of Late Devonian reefal carbonates, Canning Basin, Western Australia: confirmation of a seawater REE proxy in ancient limestones. *Geochim. Cosmochim. Acta* **68**, 263–283 (2004).
106. Maruyama, S. *et al.* The naked planet Earth: Most essential pre-requisite for the origin and evolution of life. *Geoscience Frontiers* **4**, 141–165 (2013).
107. Reinhard, C. T. *et al.* Evolution of the global phosphorus cycle. *Nature* **541**, 386 (2016).
108. Canfield, D. E., Poulton, S. W. & Marbonne, G. M. Late-Neoproterozoic deep-ocean oxygenation and the rise of animal life. *Science* **315**, 92–95 (2007).
109. Tatzel, M., von Blanckenburg, F., Oelze, M., Bouchez, J. & Hippler, D. Late Neoproterozoic seawater oxygenation by siliceous sponges. *Nature. Communications* **8**, 621 (2017).
110. Mángano, M. G. & Buatois, L. A. Decoupling of body-plan diversification and ecological structuring during the Ediacaran–Cambrian transition: evolutionary and geobiological feedbacks. *Proceedings: Biological Sciences* **281**, 1–9 (2014).
111. Han, T. M. & Runnegar, B. Megascopic eukaryotic algae from the 2.1-billion-year-old neogae iron-formation, Michigan. *Science* **257**, 232–235 (1992).
112. Johnston, D. T., Wolfe-Simon, F., Pearson, A. & Knoll, A. H. Anoxygenic photosynthesis modulated Proterozoic oxygen and sustained Earth's middle age. *Proceedings of the National Academy of Sciences* **106**, 16925–16929 (2009).
113. Goldberg, T., Strauss, H., Guo, Q. & Liu, C. Reconstructing marine redox conditions for the Early Cambrian Yangtze Platform: Evidence from biogenic sulphur and organic carbon isotopes. *Palaeogeogr. Palaeoclimatol. Palaeoecol.* **254**, 175–193 (2007).
114. Jin, C. *et al.* Spatiotemporal variability of ocean chemistry in the early Cambrian, South China. *Science China Earth Sciences* **57**, 579–591 (2014).
115. Zhang, J., Fan, T., Algeo, T. J., Li, Y. & Zhang, J. Paleo-marine environments of the Early Cambrian Yangtze Platform. *Palaeogeogr. Palaeoclimatol. Palaeoecol.* **443**, 66–79 (2016).
116. Marais, D. J. D., Strauss, H., Summons, R. E. & Hayes, J. M. Carbon isotope evidence for the stepwise oxidation of the Proterozoic environment. *Nature* **359**, 605 (1992).

Acknowledgements

This study was supported by funds from the National Natural Science Foundation of China (41873006) and the Chinese Academy of Sciences (XDB18000000). Thanks are due to Yan'an Shen, Jun Yan and Jing Huang for their assistance with field sampling and discussion, and to Ping'an Peng for his assistance with the organic carbon isotope analysis in Guangzhou.

Author Contributions

Weiping Li has undertaken this work and completed the analysis of all data. Yanyan Zhao has drafted and finished the manuscript. Mingyu Zhao has made contributions to the interpretation of data and revised it critically for important content. Xiang-Ping Zha has assisted the carbon and oxygen isotope analyses of carbonates. Yong-Fei Zheng has designed this research made substantial contributions to the conception. All authors approve this submission.

Additional Information

Supplementary information accompanies this paper at <https://doi.org/10.1038/s41598-019-47142-3>.

Competing Interests: The authors declare no competing interests.

Publisher's note: Springer Nature remains neutral with regard to jurisdictional claims in published maps and institutional affiliations.



Open Access This article is licensed under a Creative Commons Attribution 4.0 International License, which permits use, sharing, adaptation, distribution and reproduction in any medium or format, as long as you give appropriate credit to the original author(s) and the source, provide a link to the Creative Commons license, and indicate if changes were made. The images or other third party material in this article are included in the article's Creative Commons license, unless indicated otherwise in a credit line to the material. If material is not included in the article's Creative Commons license and your intended use is not permitted by statutory regulation or exceeds the permitted use, you will need to obtain permission directly from the copyright holder. To view a copy of this license, visit <http://creativecommons.org/licenses/by/4.0/>.

© The Author(s) 2019